Eurasian Journal of Physics and Functional Materials

2026, 10(1), 72-80

Structural transformations of Fe-based metallic glasses after thermal treatment and the effect of these changes on their thermal stability

N. Rafiyev[1], A. Isayeva[2,*], V. Ahmadov[2], A. Abdullayev[2], H. Huseynov[2], G. Askerova[1]

[1]Laboratory of Physics of Metals and Alloys,Azerbaijan University of Architecture and Construction, Baku, Azerbaijan

[2]Department of Physics and Chemistry, Azerbaijan University of Architecture and Construction, Baku, Azerbaijan

E-mail: aida.isayeva@azmiu.edu.az

DOI: **10.32523/ejpfm.2026100105**

Received: 01.03.2026 - after revision

The wide-ranging applications of amorphous materials are highly dependent on their thermal stability. In this study, variations in activation energy during different thermal treatment regimes of $Fe_{92}Si_6C_2$ amorphous ribbons were investigated using the DSC analysis method. The results revealed that the amorphous phase of the material transitions into various crystalline phases through a sequential formation process. Calculations based on the Ozawa method determined the activation energy to be 143 kJ/mol. This value confirms the material's high thermal stability and its suitability for operation within the temperature range of 0–100 ° C. The findings of this study provide both scientific and practical insights into understanding the behavior of amorphous materials in thermal processes and optimizing their industrial applications.

Keywords: Amorphous ribbon; metallic glass; activation energy; Ozawa model

Introduction

Metallic glass is obtained by rapidly cooling molten metal ($10^6 - 10^8$ K/s) to prevent the nucleation and growth of crystalline phases [1–3]. To obtain an amorphous structure, the main factor in the equipment is considered to be the critical cooling rate. The critical cooling rate is the cooling threshold at which the liquid, upon reaching this limit, solidifies in the amorphous state without transforming into a crystalline structure. In our process, the critical cooling rate was 10^6 K/s [4–6].

Rapid cooling results in an amorphous structure, meaning the atoms do not form the regular, periodic arrangement found in crystalline materials [7, 8]. The presence of this amorphous structure in metallic glass leads to superior mechanical, electrical, magnetic, and corrosion properties, prompting extensive research into this material [9–12]. In recent years, studies on metallic glasses have found practical applications in various fields [13–15]. They are particularly used extensively as elements in devices for the production and transmission of electrical energy [16, 17]. Metallic glasses are thermodynamically unstable materials. When heated, relaxation and crystallization processes occur [18, 19]. If metallic glass is heated below its crystallization temperature, its structure transitions to a more equilibrium state, known as structural relaxation. This is a thermally activated process that occurs below the glass transition temperature, involving the redistribution of atoms over short distances [20, 21]. Many properties change continuously, either reversibly or irreversibly, including free volume, density, magnetic properties, electrical properties, etc. [22, 23]. Amorphous metals exhibit unique thermal behaviors due to their disordered atomic structures, especially after thermal effects [24]. To analyze these behaviors, several kinetic models and equations are used, including the Mel-Johnson-Avrami-Kolmogorov (MJAK) model, Arrhenius equation, Ozawa equation, and Kissinger method. These models help understand phase transformations and calculate activation energies [25, 26].

Experimental Materials and Methods

In this study, $Fe_{92}Si_6C_2$ amorphous samples obtained by rapid cooling from the molten state were used. The amorphous nature of the samples was determined by X-ray diffraction (XRD) method. The tests were carried out using a Bruker D8 Advance XRD diffractometer with copper radiation (CuK$\alpha_1 = 1.54056$ Å) at 40 kV and 30 mA. The Kβ radiation, which could interfere with the XRD analysis, was filtered out using a graphite monochromator to ensure accurate diffraction patterns.

The DSC method was used to study the processes occurring in the samples after thermal effects. DSC analyses were conducted on a HITACHI DSC 7020 device. Various methods were employed to elucidate the thermal stability of the samples and calculate the activation energies of phase transitions. Brief descriptions of these methods are provided below.

Mehl-Johnson-Avrami-Kolmogorov (MCAK) Model: The MCAK model describes isothermal phase transformations, analyzing the formation and growth processes of crystallites. It is widely used to model the crystallization kinetics in amorphous metals. The MCAK equation is utilized to interpret differential scanning calorimetry (DSC) data, helping to determine the rates of crystallite formation and growth sizes during phase transitions [26].

Arrhenius Equation: The Arrhenius equation is crucial for understanding the temperature dependence of reaction rates. In the context of amorphous metals, it is used to model crystallization kinetics and determine activation energy for various thermal processes. The activation energy is calculated by plotting the logarithm of the reaction rate against $1/T$.

Kissinger Method: The Kissinger method involves analyzing the peak temperatures of DSC curves obtained at different heating rates. With this method, the activation energy can be calculated by plotting the logarithm of the heating rate corresponding to the inverse value of the peak temperature based on the DSC curves. This method is extensively used to study the processes occurring during the transition of metallic glasses to the crystalline state.

Ozawa Equation: The Ozawa equation is used to analyze crystallization kinetics under non-isothermal conditions. It allows for the determination of activation energies without assuming a specific kinetic model. This method is particularly advantageous for complex systems where multiple processes may occur simultaneously. Studies indicate that the relaxation behavior of metallic glasses is closely related to their free volume, impacting their plasticity and thermal stability. Research on the non-isothermal crystallization kinetics of amorphous alloys, such as nickel-phosphorus, demonstrates that the Ozawa method can effectively determine activation energies and provide extensive information about the material's crystallization process [25, 26].

Results and discussion

The amorphous structure of the samples was determined using the XRD method [26]. This technique, based on X-ray diffraction, revealed no characteristic peaks of crystals (Figure 1), confirming the amorphous nature of the samples.

Using DSC analysis values and the Ozawa method, it is possible to calculate the thermal behavior of amorphous metals and the activation energies required for their transition to a crystalline state [25, 26]. Calculations and analyses are typically performed on materials in their unprocessed state. However, during practical use, materials are subjected to certain thermal effects. Understanding the changes in activation energies after these processes, and after subsequent thermal exposure during operational periods, is of significant scientific and practical importance.

In this study, the changes in activation energy in $Fe_{92}Si_6C_2$-based samples subjected to various processing techniques were examined using the DSC analysis method. Figure 2 shows the DSC analysis results of an amorphous and unprocessed $Fe_{92}Si_6C_2$ ribbon sample.

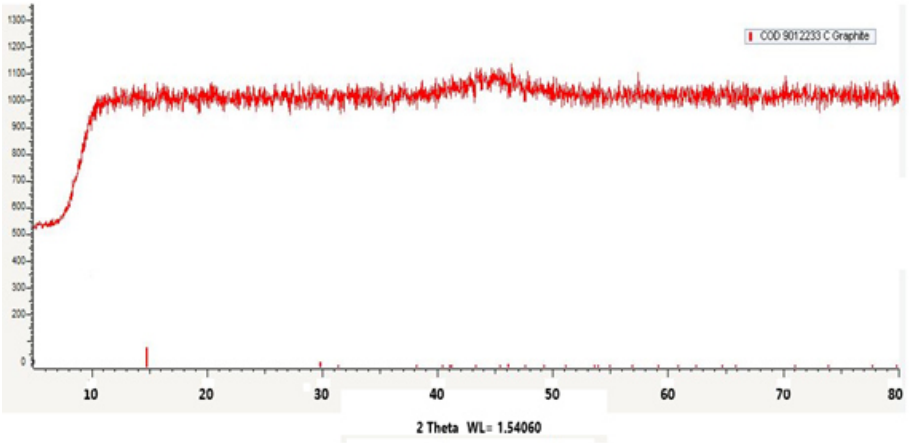

Figure 1.XRD Spectrum of $Fe_{92}Si_6C_2$ -Based Sample.

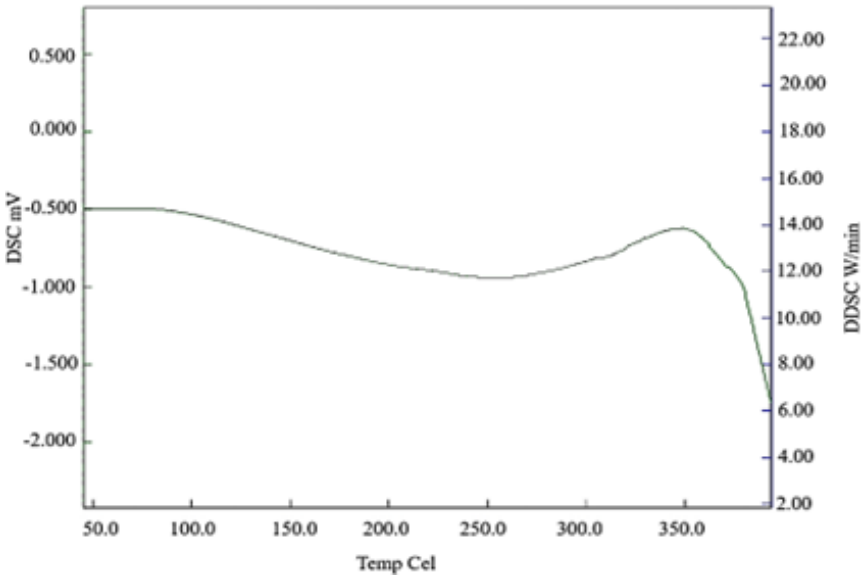

Figure 2. Initial DSC Analysis of the $Fe_{92}Si_6C_2$ Amorphous Ribbon.

The graph shows fluctuations between -2.0 mW and 0.5 mW, reflecting the material's specific heat changes, including the onset of crystallization and other thermal events. Significant thermal events such as the glass transition temperature (T_g) and the crystallization temperature (T_c) appear as distinct peaks within specific temperature ranges on the DSC graph. Notably, an exothermic reaction starts around 300° C and continues rapidly toward 350° C, indicating the onset of crystallization. Small fluctuations along the curve reflect the material's stability and potential chemical reactions. A relatively stable exothermic trend is observed from approximately 50° C to 300° C, suggesting material stability within this temperature range. Changes in the slope of the peaks indicate variations in the material's heat capacity.

In summary, this DSC graph reveals that the $Fe_{92}Si_6C_2$ amorphous ribbon exhibits a consistent thermal behavior up to around 300° C, after which it undergoes a distinct reaction attributable to crystallization or another thermal event. This analysis provides informative data to understand the thermal properties of the unprocessed material and to optimize thermal treatment processes for application.

The DSC analysis results of the amorphous sample processed at 250° C for 40 minutes are presented in Figure 3.

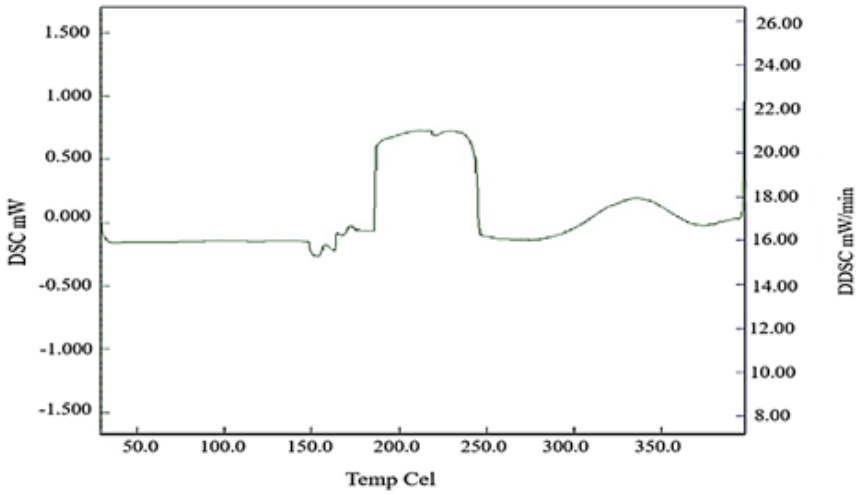

Figure 3. DSC Analysis of the $Fe_{92}Si_6C_2$ Amorphous Ribbon after Treatment at 250 ° C for 40 Minutes.

This second DSC graph illustrates the thermal behavior of the $Fe_{92}Si_6C_2$ amorphous ribbon after being held at 250° C for 40 minutes. Analyzing this graph allows us to interpret the thermal properties of the material post-treatment. Generally, regions of exothermic and exothermic reactions can be observed on the graph. A small exothermic reaction is observed around 150° C, followed by a distinct exothermic peak around 200° C. This suggests that the material undergoes a glass transition or another thermal transformation. The glass transition temperature (T_g) is the temperature at which the material changes from a rigid amorphous state to a more flexible, rubbery state, marking the onset of structural relaxation. On the DSC curve, this transition is typically observed as a subtle baseline shift rather than a pronounced exothermic peak. The more significant exothermic event around 200°C indicates the onset of partial crystallization. In this region, crystalline nuclei begin to form within the amorphous matrix, and the material gradually starts transitioning toward a more crystalline structure. Significant slope changes in the graph may reflect variations in the material's heat capacity. The prominent exothermic reaction, particularly after 200° C, indicates a substantial change in the material's heat capacity. The material appears relatively stable between approximately 50° C and 150° C. The substantial exothermic reaction starting around 180 – 200° C and continuing up to about 240 – 250° C likely indicates partial crystallization. After 250° C, a stable trend in the material's thermal behavior re-emerges, possibly indicating the completion of the initial polycrystalline phase formation process. In summary, this DSC graph reveals more detailed thermal behavior of the amorphous ribbon at this stage. A clear exothermic reaction, particularly around 200° C, suggests the onset of initial polycrystalline phase formation. The DSC analysis indicates that even after being subjected to relaxation processes by holding at 250° C for 40 minutes, the material retains its previous structure up to 150° C.

The DSC graph depicted in Figure 4 illustrates the thermal behavior of the $Fe_{92}Si_6C_2$ amorphous ribbon following thermal treatment at 350° C for 40 min-

utes.

The graph represents the relationship between heat flow (mW) and temperature ($^\circ$C). A slight exothermic trend (heat absorption) is observed in the 0° C-50° C range, which may be related to the material's stabilization and initial thermal effects. In the 50° C-250° C temperature range, the graph remains generally stable or shows a slight downward trend, indicating the absence of significant phase transitions or chemical reactions.

In the 200° C-300° C range, a minimum point around -1.5 mW is observed, corresponding to the glass transition temperature (T_g) of the $Fe_{92}Si_6C_2$ amorphous ribbon. The glass transition temperature is associated with structural changes in the amorphous phase. An exothermic peak is observed in the 300° C–350° C range, signaling the onset of crystallization or other significant phase transitions. At this peak, the heat flow increases, indicating heat absorption. Beyond 350° C, a decline in the graph's slope is noted, which may indicate the completion of crystallization or other phase transitions. This graph illustrates the thermal stability of $Fe_{92}Si_6C_2$ amorphous ribbons after thermal treatment: The identification of the glass transition temperature (approximately 200° C) reflects the internal stability of the amorphous phase and its compatibility with operational conditions. Crystallization processes occurring above 300° C highlight the material's sensitivity to thermal effects outside its operational range. The results demonstrate that $Fe_{92}Si_6C_2$ ribbons exhibit thermal stability in the $0-100^\circ$ C range, making them a suitable candidate for industrial applications.

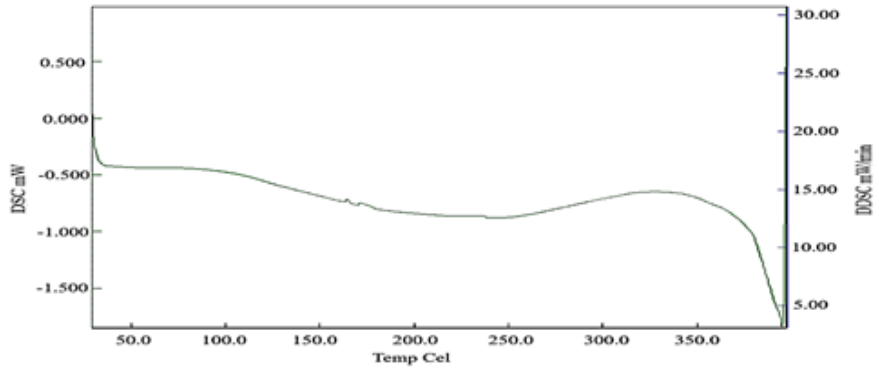

Figure 4. DSC Analysis of the $Fe_{92}Si_6C_2$ Amorphous Ribbon After Thermal Treatment at 350 $^\circ$ C for 40 Minutes.

To calculate the activation energy, the Ozawa method is considered the most suitable among the methods listed above [25, 26]. This method allows the determination of activation energies without assuming a specific kinetic model. Using the Ozawa method, it is possible to calculate the activation energy from DSC data obtained at different temperatures. Calculating the activation energy requires values of heating rates (β) measured at several different temperatures. According to the Ozawa method, the basic formula for calculating the activation energy (E) is given as follows:

$$\log(\beta) = \log(A) - \frac{E}{2.303R}\frac{1}{T}$$

where B – heating rate, A – Arrhenius constant, E – activation energy, R – universal gas constant, T – absolute temperature. The necessary data for calculating the activation energy, such as the temperatures (T_{p}) corresponding to the maximum values for four different heating rates (β), are provided in Table 1.

Table 1.
Peak temperatures (T_p) at different heating rates (β) used for activation energy calculation.

No.	Heating Rate β (°C/min)	Peak Temperature T_{p} (°C)
1	5	325
2	10	335
3	15	345
4	20	350

The process involves the following steps: conversion of temperature data to Kelvin ($T(\mathrm{K}) = T(^{\circ}\mathrm{C}) + 273.15$), calculation of the logarithm of the heating rate ($\log(\beta)$), calculation of the inverse temperature ($1/T(\mathrm{K})$), and plotting the graph. A plot of $\log(\beta)$ against $1/T$ is created (Figure 5).

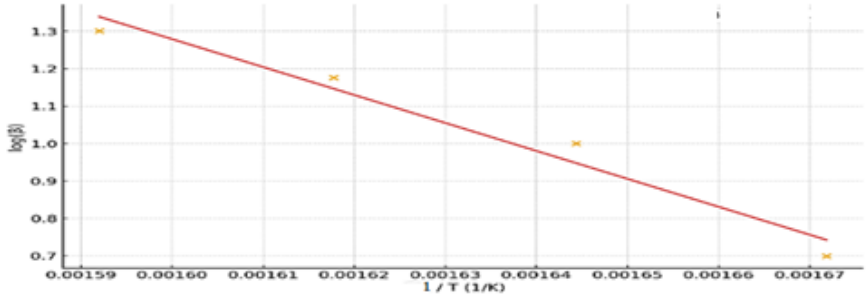

Figure 5. Plot of Logarithm of Heating Rate vs. Inverse Temperature (Ozawa Coordinates).

From the slope of the graph, the activation energy (E) is calculated. The calculation using the Ozawa method results in an activation energy (E) value of 142.998 kJ/mol ($\sim$ 143 kJ/mol). This value indicates the activation energy of the $Fe_{92}Si_6C_2$ –based amorphous sample and is an important parameter for understanding the sample's thermal behavior, confirming its substantial thermal stability during practical use.

Potential application areas of $Fe_{92}Si_6C_2$ amorphous ribbons. Industrial applications of $Fe_{92}Si_6C_2$ ribbons:

The high thermal stability of $Fe_{92}Si_6C_2$ ribbons makes them suitable for use in energy transmission and distribution systems, particularly in transformer cores [27].

The amorphous structure of the materials enhances their magnetic properties, improving energy efficiency and reducing energy losses.

Applications in electronics: The high magnetic permeability of $Fe_{92}Si_6C_2$ ribbons makes them ideal for use in electromagnetic shielding materials and sensors [28].

The elevated glass transition temperature enables their application in electronic devices requiring stability under high-temperature conditions.

Mechanical properties and durability applications: With high thermal stability and mechanical robustness, these ribbons can serve as alternative materials for high-performance magnetic devices [29].

Potential applications in the automotive industry: Lightweight and high-performance amorphous ribbons hold promise for use in electric motors and energy recovery systems in the automotive industry [30].

Conclusion

1. In this study, the thermal behavior and changes in activation energy of $Fe_{92}Si_6C_2$ amorphous ribbons under different thermal treatment regimes were investigated. The results of DSC analyses revealed that the amorphous phase undergoes a stepwise transition into various crystalline phases due to thermal treatment. Calculations based on the Ozawa method indicated that the activation energy is 143 kJ/mol, confirming the material's high thermal stability within its operational temperature range (0 °C–100 °C).

2. This research provides fundamental insights into the thermal stability of amorphous materials. The high activation energy of the material demonstrates its suitability for industrial applications, particularly in energy generation and transmission systems. Additionally, the findings contribute to understanding the crystallization kinetics of amorphous ribbons and provide a basis for optimizing their thermal treatment processes. This information opens up potential opportunities to enhance the technical properties of amorphous materials and identify new application areas.

Acknowledgement

This work was supported by the Azerbaijan Science Foundation - Grant No. AEF–MQM–QA–2–2023–3(45)–05/01/1–M–01.

References

[1] R. Hasegawa, Journal of Magnetism and Magnetic Materials **304** (2006) 187–191. [*CrossRef*]
[2] A. Inoue, A. Takeuchi, Acta Materialia **59** (2011) 2243–2267. [*CrossRef*]
[3] S. Guo, Y. Liu, Journal of Non-Crystalline Solids **358** (2012) 2753–2758. [*CrossRef*]
[4] R.K. Roy et al., Journal of Materials Science: Materials in Electronics (2023). [*CrossRef*]
[5] P. Murugaiyan et al., Journal of Superconductivity and Novel Magnetism **37** (2024) 1635–1646 . [*CrossRef*]
[6] R. Louvier et al., Key Engineering Materials **876** (2021) 25–30. [*CrossRef*]
[7] H. Koshiba, A. Inoue, A. Makino, Journal of Applied Physics **85** (1999) 5136–5138. [*CrossRef*]

[8] V.I. Ahmadov et al., Advanced Physical Research **7**(1) (2025) 133–149. [*CrossRef*]
[9] X. Zhang et al., Journal of Alloys and Compounds **1005** (2024) 176172. [*CrossRef*]
[10] S. Zhang et al., EPJ Applied Physics **98** (2023) 11. [*CrossRef*]
[11] Y. Wu et al., Intermetallics **166** (2024) 108174. [*CrossRef*]
[12] A. El Boubekri et al., Journal of Magnetism and Magnetic Materials **641** (2026) 173848. [*CrossRef*]
[13] N.M. Rafiyev, Zeitschrift fur Naturforschung A **77** (2022) 2–8. [*CrossRef*]
[14] N.M. Rafiyev, V.I. Ahmadov, A.A. Isayeva, Ukrainian Journal of Physics **68** (2023) 201–209. [*Web Link*]
[15] A.P. Abdullayev, V.I. Ahmadov, A.A. Isayeva, International Journal of Modern Physics B **35** (2021) 2150045. [*CrossRef*]
[16] D. Cao et al., Materials **18** (2025) 4637. [*CrossRef*]
[17] N. Rafiyev, A. Isayeva, V. Ahmadov, Zeitschrift fur Naturforschung A **80** (2025) 461–468. [*CrossRef*]
[18] M. Churyukanova et al., Journal of Magnetism and Magnetic Materials **492** (2019) 165598. [*CrossRef*]
[19] P. Ohodnicki et al., Journal of Alloys and Compounds **835** (2020) 155038. [*CrossRef*]
[20] A.A. Isayeva et al., Moscow University Physics Bulletin **80** (2025) 601–605. [*CrossRef*]
[21] A. Isayeva, V. Ahmadov, N. Rafiyev, Brazilian Journal of Physics **56** (2026) 29. [*CrossRef*]
[22] S. Wang et al., Advances in Materials Science and Engineering (2015) 410830. [*CrossRef*]
[23] A. Abdullayev et al., Radiation Physics and Chemistry **235** (2025) 112883. [*CrossRef*]
[24] Z.Z. Yang, L. Zhu, S.S. Jiang, Journal of Alloys and Compounds **904** (2022) 164067. [*CrossRef*]
[25] M. Tian et al., Journal of Thermal Analysis and Calorimetry **148** (2023) 1959–1970. [*CrossRef*]
[26] D. Janovszky et al., Journal of Thermal Analysis and Calorimetry **147** (2022) 7141–7157. [*CrossRef*]
[27] X. Huang et al., Scientia Sinica: Physica, Mechanica et Astronomica **55**(8) (2025) 286108. [*CrossRef*]
[28] S.F. Samadov et al., Journal of Materials Science **61** (2026) 4668–4682. [*CrossRef*]
[29] A.P. Abdullayev et al., Modern Physics Letters B **40** (2026) 2550273. [*CrossRef*]
[30] T.M. Panakhov et al., Technical Physics **64** (2019) 987–989. [*CrossRef*]